Quantum Electronics **49** (4) 344–349 (2019)

https://doi.org/10.1070/QEL16966

Effect of group velocity dispersion on femtosecond filamentation of Bessel–Gaussian beams

S.V. Chekalin, V.O. Kompanets, E.D. Zaloznaya, V.P. Kandidov

Abstract. **Laser colouration technique is employed to investigate the structures of colour centres induced in an isotropic LiF crystal by Bessel–Gaussian and Gaussian beams in the single-pulse filamentation regime. Femtosecond laser pulses at radiation wavelengths corresponding to zero (1250 nm) and anomalous (1900 nm) group velocity dispersions were focused into the sample using an axicon or a spherical lens. As shown experimentally and numerically, with increase in radiation energy the length of the structure of colour centres (or the plasma channel length) increases in the domain of zero group velocity dispersion but remains invariable under conditions of anomalous dispersion, when there emerge light bullets. The path length of the light bullets amounts to about 200 μm and does not depend on the pulse energy and the way of focusing, which confirms their robustness.**

Keywords: *light bullet, Bessel–Gaussian beam, femtosecond filamentation, laser colouration technique, group velocity dispersion.*

1. Introduction

The term 'light bullets' (LBs) was introduced for self-consistent nonlinear excitations with a high localisation of the light field. Silberberg [1] formulated the conception of LB formation in the combined and self-consistent compression of laser radiation both in space and in time under the self-action of a wave packet in a dispersion medium with a cubic nonlinearity. The mechanism of LB formation is based on two effects: anomalous group velocity dispersion (AGVD) and Kerr nonlinearity [2–5]. The phase self-modulation due to the Kerr nonlinearity gives rise to a nonlinear positive pulse chirp (a long-wavelength shift at the leading edge and a short-wavelength shift at the trailing one). In the AGVD, the higher frequencies have higher group velocities, so that the trailing edge moves faster than the leading one. This results in the effective pulse shortening down to one optical cycle, an increase in its peak intensity up to figures of the order of 10^{14} W cm^{-2}, and the formation of a light bullet. The high intensity is responsible for plasma production, which abruptly cuts off the trailing edge of the bullet due to defocusing. Under AGVD conditions, this strongly broadens the LB spectrum to the short-wavelength side and forms an isolated anti-Stokes supercontinuum (SC) wing [6–10]. Increasing the initial pulse energy is responsible for the formation of new LBs accompanied with the ejection of fixed SC portions in the anti-Stokes wing domain by each bullet [11]. It is noteworthy that the appearance of a sequence of LBs is due to compression not only in space but also in time, unlike the refocusing observed in the case of normal group velocity dispersion (GVD).

The localisation of the light field in the volume of uniform and isotropic media with cubic nonlinearity and the formation of an LB approximately two optical cycles in duration were first observed in our paper [12] in the measurement of the autocorrelation function of the LBs in the filamentation of femtosecond pulses in fused silica at a wavelength $\lambda = 1900$ nm, which lies in the AGVD domain. In these experiments, the LB path length did not exceed several millimetres, which was estimated from the plasma channel length in the photograph of the luminous track. Evaluation of the LB path length from the photographs of the luminous tracks of plasma channels and the scattered light of the visible part of the SC was used in many works [13–17]. However, the brightness of these tracks is so low that exposing to several thousand pulses is required to photograph these tracks. Pulse-to-pulse fluctuations of laser parameters entail significant errors in the resultant information.

This problem was overcome employing laser colouration technique [18], which made it possible, first, to carry out the measurements without signal accumulation, i.e. using only one laser pulse, and second, without any inaccuracies that arise from the overlap of the radiations of the SC, conical emission, and the plasma channel. Chekalin et al. [19] employed this technique to record for the first time the LBs approximately one light oscillation cycle in duration and less than 10 μm in diameter as well to unambiguously measure their path length, which does not exceed 0.5 mm. In the laser colouration technique, the dynamics of LB origination and development in the filamentation of single femtosecond mid-IR pulses in LiF is investigated by the density variation of long-lived colour centres (CCs), which originate in the light field due to multiphoton processes in the resultant filament. In this case, the long-lived structures made up of CCs, which are produced by only one laser pulse, may be easily detected and investigated under subsequent continuous laser illumination in their absorption band near 450 nm. This permits the three-dimensional structure of the optical field of an LB to be comprehensively investigated along its entire path in the material with a spatial resolution higher than 1 μm (defined exclusively by the resolving power of the microscope in use).

S.V. Chekalin, V.O. Kompanets Institute for Spectroscopy, Russian Academy of Sciences, ul. Fizicheskaya 5, 108840 Moscow, Troitsk, Russia; e-mail: chekalin@isan.troitsk.ru;
E.D. Zaloznaya, V.P. Kandidov Institute for Spectroscopy, Russian Academy of Sciences, ul. Fizicheskaya 5, 108840 Moscow, Troitsk, Russia; Faculty of Physics and International Laser Center, M.V. Lomonosov Moscow State University, Vorob'evy gory, 119991 Moscow, Russia; e-mail: ed.zaloznaya@physics.msu.ru

Received 7 February 2019
Kvantovaya Elektronika **49** (4) 344–349 (2019)
Translated by E.N. Ragozin

In the present work, the laser colouration technique is used to investigate the LBs produced by focusing a Gaussian beam of femtosecond radiation in LiF with an axicon. It is pertinent to note that practically all works on the filamentation of laser radiation focused with an axicon were performed in conditions of normal GVD, when LBs do not spring up. Polynkin et al. [20] observed a six-fold lengthening of the plasma channel in the air when an axicon was employed to focus a 50-fs long $\lambda = 800$ nm radiation pulse instead of an ordinary lens. The advantages of using conical focusing in lieu of the ordinary lens focusing in the case of normal GVD were also emphasised in the numerical investigation outlined in Ref. [21]: focusing a Gaussian beam with an axicon results in the formation of a plasma channel of greatest length with a uniform electron density distribution.

In experiments on the filamentation in K-108 glass for pulses whose power exceeded the critical power of self-focusing by two orders of magnitude, the use of axicon focusing made it possible to avoid multiple filamentation, whose threshold is significantly lower in the case of a spherical lens, and to obtain a long filament after several refocusings [22, 23]. As a result, instead of a speckle pattern produced in the conical emission in the case of multiple filamentation for lens focusing, it was possible to observe a regular system of concentric rings, which testified that the SC sources in the filament were immune to small fluctuations of the pulse parameters for axicon focusing.

Faccio et al. [24] also observed an increase in multiple filamentation threshold in the focusing of a 40-fs long $\lambda = 800$ nm Gaussian beam in water with an axicon with an angle of 20° at the base in comparison with the focusing with a lens of the same numerical aperture. Dubietis et al. [25] investigated the effect of axicon's position relative to the sample. In Refs [26–28], the focusing of femtosecond $\lambda = 800$ nm subterawatt radiation pulses in a transparent dielectric target using an axicon with a 20°–30° base angle was used to lengthen the path of nonlinear optical radiation–medium interaction. Employing a 40-fs long $\lambda = 800$ nm pulse, whose power was several orders of magnitude higher than the critical self-focusing power, Krithika et al. [29] investigated experimentally how the regime of filamentation in a 15-mm long BaF_2 depended on the axicon base angle. An analysis of the luminous channels photographed from the side suggested that lowering the base angle from 7.5° to 1° resulted in a significant increase in filament formation threshold and an increase of the distance between the self-focusing points in the quasi-periodic channel structure. A comparative analysis of the SC spectra obtained by focusing a 130-fs $\lambda = 800$ nm radiation pulse in a 3-mm long sapphire crystal using an axicon with a base angle of 2°18″ and a lens with a focal distance of 50 mm [30] showed their nearly complete identity.

In conditions of AGVD, the filamentation of Besselian beams and the features of LB formation for axicon focusing were studied only in our works [16, 17], in which we studied experimentally and numerically the plasma channels and the visible SC band in the filamentation of $\lambda = 800$ and 1800 nm radiation in fused silica, the focusing being performed by a quartz axicon with a base angle of 0.5°. The recombination radiation of the laser-produced filament plasma and the SC emission scattered in the sample were recorded with a digital camera through its side face. For a reliable recording, the pulse power was maintained at a level of several tens and hundreds of critical self-focusing powers and the exposure of the photographs at a level of 10^3 laser pulses. The lengths of plasma channels and filaments, which were determined from the resultant photographs, amounted to over 10 cm. The energy emission to the visible part of the SC in the LB formation was found to be the same for axicon and lens focusing, which testifies to the spectral stability of LBs. However, owing to significant errors in the determination of the plasma channel length for multiple pulse exposure, no adequate comparison was made between the LB path lengths in the filaments produced by Besselian and Gaussian beams.

The present work is concerned with the investigation of filamentation and LB formation in LiF in the axicon and lens focusing of the Gaussian beam of $\lambda = 1250$ and 1900 nm femtosecond radiations, which correspond to zero and anomalous GVD: experimentally with the use of laser colouration technique and numerically under the slowly varying wave approximation.

2. Formulations of the experiment and numerical model

The luminescent tracks of CCs in an isotropic LiF crystal were produced by alternate use of an axicon and a lens to focus the radiation at the wavelengths corresponding to the zero (1250 nm) and anomalous (1900 nm) GVD. In the experiment, use was made of a laser radiation source based on a Tsunami (a Ti:sapphire laser) femtosecond oscillator with a Millenia Vs cw solid-state pump laser, a Spitfire Pro regenerative amplifier pumped with an Empower 30 solid-state laser, and a TOPAS tuneable parametric amplifier. The half-amplitude duration of the pulses at $\lambda = 1250$ and 1900 nm was equal to 60 and 70 fs, respectively. The pulse repetition rate was equal to 1 kHz. The pulse energy was measured with a Fieldmax sensor with a PS-10 detector and varied in the experiments from 5 to 100 μJ.

With the use of a thin CaF_2 lens with a focal length $F =$ 30 cm, the radiation was focused inside the sample at a distance of several millimetres from its input face. In the focusing with an axicon with a base angle $\alpha = 0.5°$, the distance from its vertex to the input face of the 35-mm long LiF crystal was selected so as to minimise the SC generation threshold and was equal to 85 and 123 mm for the $\lambda = 1250$ and 1900 nm, respectively. When writing the CCs in the single-pulse exposure regime, after every pulse the sample was shifted in the direction perpendicular to the laser beam. To obtain the single-filament regime, when changing the wavelength the pulse energies were so varied that their peak power was only slightly higher than the critical self-focusing power. Furthermore, the energy was varied by factors of 3–5 in the irradiation of the sample. When focusing with the lens, the radiation pulse energy W at $\lambda = 1250$ and 1900 nm varied from 5 to 15 μJ and from 7 to 25 μJ, respectively. When focusing with the axicon, the energy was higher by more than three times. The employment of laser colouration technique made it possible to obtain data in single-pulse filamentation regime. In this case, the peak power was 2–8 times higher than the critical self-focusing power for the $\lambda = 1250$ nm radiation and 3–8 times higher for the $\lambda = 1900$ nm radiation, which is significantly lower than in Refs [16, 17].

To analyse the spatial luminescence intensity distribution for the recorded CCs, which reproduces the density of laser-induced electronic excitations in the filamentation in LiF, use was made of optical microscopy techniques with illumination at the wavelength of absorption by these CCs. To qualitatively analyse the written structure of the CCs, advantage was

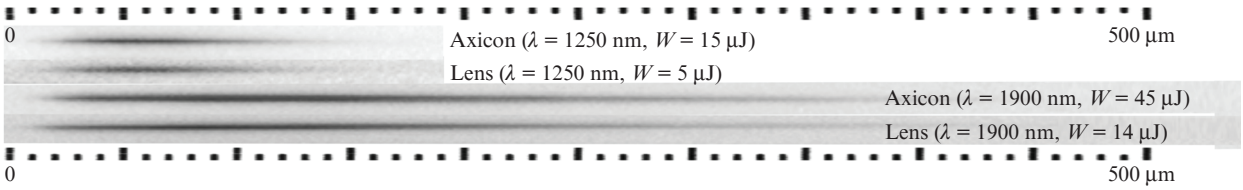

Figure 1. Luminescence of the colour centres induced in LiF in the single-pulse filamentation regime for $\lambda = 1250$ and 1900 nm radiation pulses in the lens and axicon focusing into the sample.

taken of a Euromex Oxion 5′ microscope with a cw laser illumination at $\lambda = 450$ nm and the luminescence detection with a Nikon D800 digital camera. The scattered exciting radiation was rejected with an auxiliary yellow-green light filter. The photographs of the luminescent structures induced in LiF are exemplified in Fig. 1.

To investigate the filamentation in LiF numerically, we employed the slowly varying wave approximation, using which it is possible to describe the propagation and transformation of a wave packet of duration down to one optical cycle. The equations of the mathematical model under consideration describe the beam diffraction, the pulse dispersion, the transient variations of the refractive index of the medium caused by the Kerr and plasma nonlinearities, the generation of laser plasma, and the radiation attenuation due to photoionisation and inverse bremsstrahlung.

The parameters taken in the numeral filamentation simulation were close to the experimental ones. In the axicon focusing, the light field amplitude A at the input face of the sample was defined in the form

$$A(r,t,z=0) = A_0 \exp\left[-\frac{r^2}{2a_0^2} - \frac{t^2}{2\tau_0^2} + \mathrm{i}\varphi(r)\right], \quad (1)$$

where a_0 and $2\tau_0$ are the beam radius and the duration of the Gaussian wave packet at the e^{-1} intensity level; A_0 is the amplitude of the light field. The spatial modulation of the phase φ produced by the axicon is described by the expression

$$\varphi(r) = kr(n_{ax} - 1)\alpha, \quad (2)$$

where k is the wavenumber and n_{ax} is the refractive index of the axicon material.

The results of numerical calculation of the light field amplitude in the Bessel–Gaussian beam formation in the case of axicon focusing of the Gaussian beam corresponded to the intensity distributions measured at several distances from the axicon. Figure 2 shows the radial beam intensity profiles at the distance corresponding to the position of the input face of the LiF sample for the $\lambda = 1250$ nm radiation.

For the Bessel–Gaussian beam, the central peak intensity is much higher than the intensity of the concentric rings that encompass it (Fig. 2). The femtosecond filamentation of this beam is therefore determined by the power contained in its central lobe P_{lobe}. For an estimate it may be assumed that the filamentation originates in the central lobe, whose power P_{lobe} exceeds the critical stationary self-focusing power P_{cr} of a Gaussian beam. The relative power P_{lobe}/P_{cr} at the input face

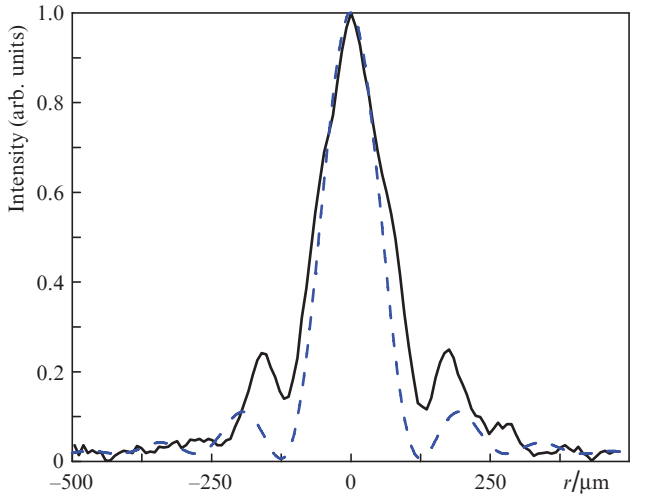

Figure 2. Radial intensity profiles of the Bessel–Gaussian beam at the input face of the LiF sample in the axicon focusing of the $\lambda = 1250$ nm radiation. The solid curve is the result of the experiment, and the dashed curve shows the numerical simulation.

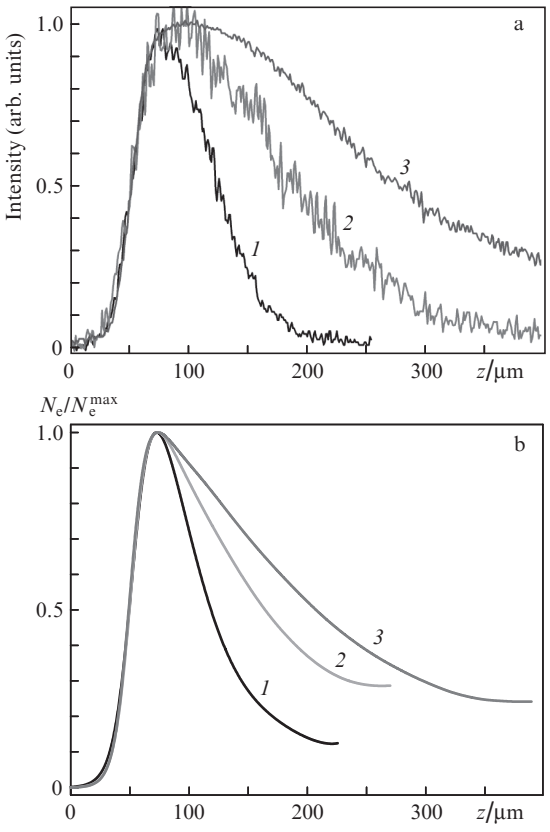

Figure 3. (a) Measured intensities of induced CC luminescence and (b) simulated electron density distributions $N_e(z)$ along the filament axis in LiF in the regime of single-pulse filamentation of femtosecond $\lambda = 1250$ nm radiation pulses focused with the axicon for a pulse energy $W = (1)$ 15, (2) 30 and (3) 42 μJ.

of the LiF crystal, which was contained in the central lobe of the Bessel–Gaussian beam and calculated from the radial intensity profile, amounted to 2–8 in all cases considered and corresponded to the regime of single filamentation.

In numerical simulation, we determined the electron density distribution along the filament axis in the plasma, which was induced in the filamentation and LB formation, as well as the spatiotemporal radiation intensity distribution at characteristic distances. The CCs originate due to the nonlinear photoexcitation of the electron subsystem of the material with the production of excitons and electron–hole pairs by way of avalanche, tunnel, and multiphoton ionisation, as well as due to direct exciton excitation [31–33]. The energy gap in LiF is close to the energy of the exciton absorption band [34], and the electron density distribution in the multiphoton generation of free carriers determines the density of induced CCs. That is why the electron density distribution along the filament axis obtained in numerical simulations reproduces the CC density distribution measured from the luminescence signal.

3. Results and their discussion

Figures 3a and 4a show the CC luminescence intensity distributions measured along the filament axis. These CCs were induced in the regime of single-pulse filamentation in LiF, with the variation of λ = 1250 and 1900 nm radiation pulse energies in the case of axicon focusing. Figures 3b and 4b show the simulated on-axis electron densities $N_e(z)$ normalised to the peak value N_e^{max}. As one can see, in the filamentation of λ = 1250 nm radiation (Fig. 3) in conditions of zero GVD the lengths of induced CC structure and the plasma channel increase with pulse energy.

With an increase in pulse energy W from 15 to 42 μJ, the experimentally measured length of the CC structure induced by the λ = 1250 nm radiation increases from 70 to 230 μm (Fig. 3a), while the length obtained by numerical simulations increases from 70 to 160 μm (Fig. 3b). However, for the λ = 1900 nm radiation under AGVD (Fig. 4) the structure and plasma channel lengths remain invariable with increasing energy W from 23 to 80 μJ. The experimentally measured channel length was equal to 220 ± 10 μm and the calculated one was equal to 190 ± 10 μm. Despite of the incomplete quantitative agreement between the experimental and numerical data, both methods of investigation demonstrate with certainty that the type of GVD has a significant effect on the length of the high light-field energy density domain in the filament and that the length of this domain, under AGVD, is independent of the pulse energy. This conclusion is borne out by the results of experiments on writing CC structures in the filamentation of the pulses focused into the LiF sample with the lens (Fig. 5).

In this case, the length of the CC structures written with the filament lengthens from 78 to 180 μm with increasing W from 5 to 15 μJ for λ = 1250 nm but remains invariable and equal to 210 ± 15 μm with increasing λ = 1900 nm pulse energy in the AGVD regime (Fig. 5). This quantity, which corre-

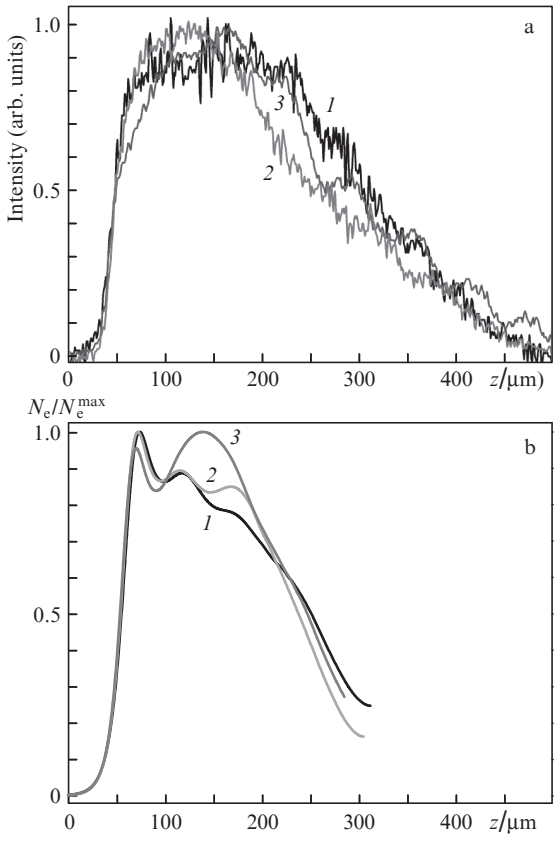

Figure 4. (a) Measured intensities of induced CC luminescence and (b) simulated electron density distributions $N_e(z)$along the filament axis in LiF in the regime of single-pulse filamentation of femtosecond λ = 1900 nm radiation pulses focused with the axicon for a pulse energy W = (*1*) 23, (*2*) 45 and (*3*) 80 μJ.

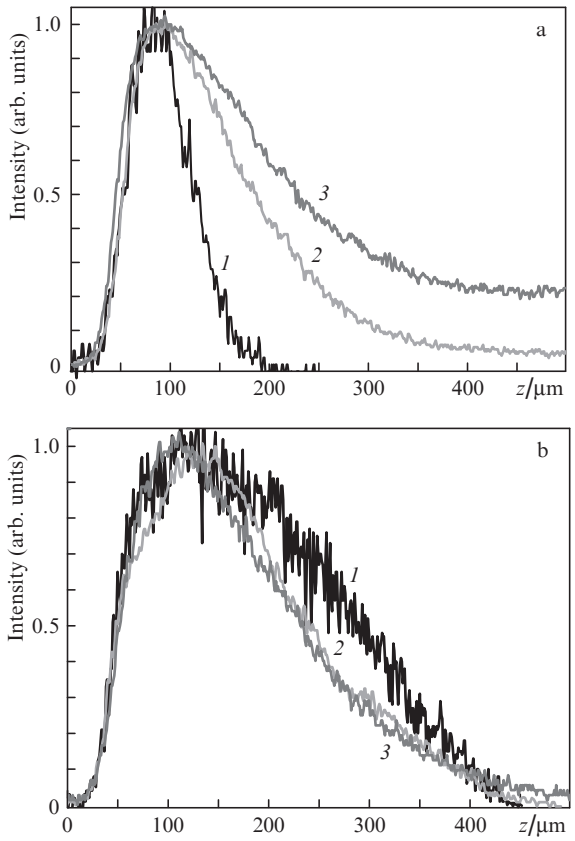

Figure 5. Luminescence intensity profiles of the CCs induced in LiF in the single-pulse filamentation of femtosecond pulses focused with a lens with a focal distance $F \approx$ 30 cm for (a) W = (*1*) 5, (*2*) 10 and (*3*) 15 μJ, λ = 1250 nm and (b) W = (*1*) 7, (*2*) 14 and (*3*) 25 μJ, λ = 1900 nm.

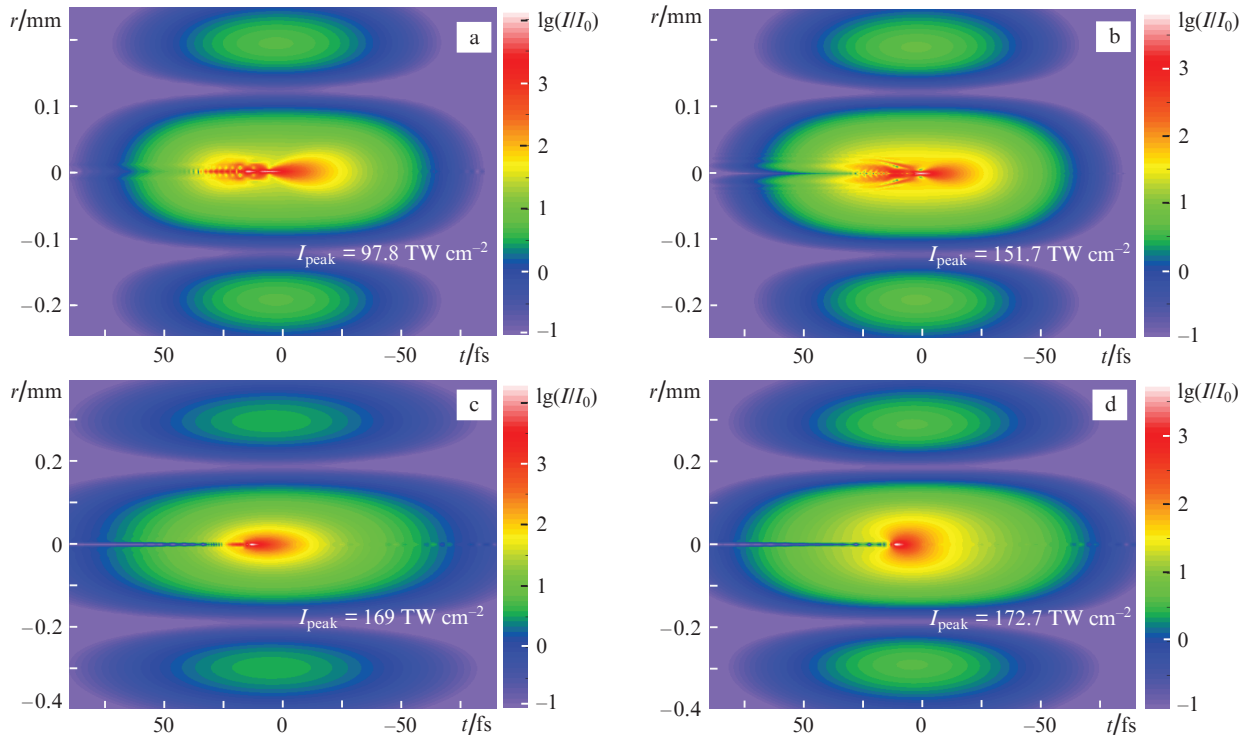

Figure 6. (Colour online) Spatiotemporal intensity distributions $I(r, t)$ of the central lobe of the Bessel–Gaussian beam of femtosecond radiation calculated for the distances at which the on-axis electron density reaches its maximum. W = (a) 15, (b) 42, (c) 23 and (d) 80 μJ, λ = (a, b) 1250 and (c, d) 1900 nm. The ring that encompasses the central lobe is represented in the distribution $I(r, t)$ by local maxima at r_0.

sponds to the LB path length, is precisely the same as for axicon focusing (Fig. 4a).

The CC structure and plasma channel lengths are independent of the input pulse energy in the filamentation under AGVD, because a high-intensity LB is formed, which is attended with CC and plasma production in its path length. Since LBs originate due to the self-organisation of the light field in a nonlinear dispersive medium, their characteristics are determined by the radiation wavelength and the nonlinear optical material properties and are independent of the pulse energy and focusing conditions. Figure 6 shows the simulated spatiotemporal intensity distributions $I(r,t)$ in the central lobe of the Bessel–Gaussian beam of the λ = 1250 and 1900 nm radiation at the distances at which the electron density $N_e(z)$ attains its maximum.

As one can see, for the zero GVD (λ = 1250 nm) the $I(r = 0, t)$ distribution and the peak intensity I_{peak} depend on the driving pulse energy. While for a radiation energy W = 15 μJ the intensity I_{peak} does not exceed 100 TW cm^{-2}, for W = 42 μJ it becomes higher than 150 TW cm^{-2}. In this case, the pulse duration defined as the full width at half height of the on-axis distribution $I(r = 0, t)$ shortens from 13 to 4.3 fs. In the case of AGVD, irrespective of the pulse energy the peak intensity $I_{peak} = 171 \pm 2$ TW cm^{-2} and the pulse duration is equal to 2 fs. Therefore, for the zero GVD the radiation compression takes place only with increasing radiation energy. For AGVD, the radiation gives rise to a LB, whose parameters are independent of the pulse energy.

4. Conclusions

With increasing the energy of the femtosecond radiation focused in LiF with a lens or an axicon, the lengths of the CC structure and the plasma channel induced in the filament become longer for the zero GVD. For AGVD, the CC structure length, which is equal to the path length of the generated LB, is independent of the pulse energy, is the same for Gaussian and Bessel–Gaussian beams, and is no longer than 200 μm. The real LB path length recorded by laser colouration technique in the single-pulse regime is two orders of magnitude shorter than the path length measured in the multiple-pulse regime from the plasma channel and scattered SC lengths. The light bullet is a stable formation produced in a nonlinear dispersive medium in the filamentation of Gaussian and Bessel–Gaussian beams of femtosecond radiation, and its parameters are determined by the radiation wavelength and the nonlinear optical characteristics of the medium. The resultant data bear out the conclusion about spectral LB robustness formulated in Refs [35, 36] proceeding from the energy measurements of the anti-Stokes wing of its spectrum.

Acknowledgements. Our experiments were carried out on the unique research facility "Multiple-purpose femtosecond laser diagnostic spectrometric complex" of the Institute for Spectroscopy of the Russian Academy of Sciences. The theoretical investigation was supported by the Russian Science Foundation (Project No. 18-12-00422) and the experimental investigation was supported by the Presidium of the Russian Academy of Sciences (Fundamental Research Programme "Extreme Light Fields and Their Interaction with Matter").

References

1. Silberberg Y. *Opt. Lett.*, **15**, 1282 (1990).
2. Berge L., Skupin St. *Phys. Rev. Lett.*, **100**, 113902 (2008).

3. Smetanina E.O., Kompanets V.O., Chekalin S.V., Kandidov V.P. *Quantum Electron*., **42**, 913 (2012) [*Kvantovaya Elektron*., **42**, 913 (2012)].
4. Smetanina E.O., Kompanets V.O., Chekalin S.V., Kandidov V.P. *Quantum Electron*., **42**, 920 (2012) [*Kvantovaya Elektron*., **42**, 920 (2012)].
5. Smetanina E.O., Dormidonov A.E., Kandidov V.P. *Laser Phys*., **22**, 1189 (2012).
6. Smetanina E.O., Kompanets V.O., Chekalin S.V., Dormidonov A.E., Kandidov V.P. *Opt. Lett*., **38**, 16 (2013).
7. Durand M., Lim K., Jukna V., McKee E., Baudelet M., Houard A., Richardson M., Mysyrowicz A., Couairon A. *Phys. Rev. A*, **87**, 043820 (2013).
8. Vasa P., Dharmadhikari J.A., Dharmadhikari A.K., Sharma R., Singh M., Mathur D. *Phys. Rev. A*, **89**, 043834 (2014).
9. Dormidonov A.E., Kompanets V.O., Chekalin S.V., Kandidov V.P. *Opt. Express*, **23**, 29202 (2015).
10. Dharmadhikari J.A., Deshpande R.A., Nath A., Dota K., Mathur D., Dharmadhikari A.K. *Appl. Phys. B*, **117**, 471 (2014).
11. Chekalin S.V., Kompanets V.O., Dokukina A.E., Dormidonov A.E., Smetanina E.O., Kandidov V.P. *Quantum Electron*., **45**, 401 (2015) [*Kvantovaya Elektron*., **45**, 401 (2015)].
12. Chekalin S.V., Kompanets V.O., Smetanina E.O., Kandidov V.P. *Quantum Electron*., **43**, 326 (2013) [*Kvantovaya Elektron*., **43**, 326 (2013)].
13. Smetanina E.O., Kompanets V.O., Dormidonov A.E., Chekalin S.V., Kandidov V.P. *Laser Phys. Lett*., **10**, 105401 (2013).
14. Majus D., Tamošauskas G., Gražulevičiūtė I., Garejev N., Lotti A., Couairon A., Faccio D., Dubietis A. *Phys. Rev. Lett.*, **112**, 193901 (2014).
15. Durand M., Jarnac A., Houard A., Liu Y., Grabielle S., Forget N., Durecu A., Couairon A., Mysyrowicz A. *Phys. Rev. Lett*., **110**, 115003 (2013).
16. Chekalin S.V., Dokukina A.E., Smetanina E.O., Kompanets V.O., Kandidov V.P. *Quantum Electron*., **44**, 570 (2014) [*Kvantovaya Elektron*., **44**, 570 (2014)].
17. Dokukina A.E., Smetanina E.O., Kompanets V.O., Chekalin S.V., Kandidov V.P. *Proc. SPIE*, **9219**, 92190I (2014).
18. Kuznetsov A.V., Kompanets V.O., Dormidonov A.E., Chekalin S.V., Shlenov S.A., Kandidov V.P. *Quantum Electron*., **46**, 379 (2016) [*Kvantovaya Elektron*., **46**, 379 (2016)].
19. Chekalin S.V., Kompanets V.O., Dormidonov A.E., Kandidov V.P. *Quantum Electron*., **48**, 372 (2018) [*Kvantovaya Elektron*., **48**, 372 (2018)].
20. Polynkin P., Kolesik M., Roberts A., Faccio D., Di Trapani P., Moloney J. *Opt. Express*, **16**, 15733 (2008).
21. Kosareva O.G., Grigor'evskii A.V., Kandidov V.P. *Quantum Electron*., **35**, 1013 (2005) [*Kvantovaya Elektron*., **35**, 1013 (2005)].
22. Chekalin S.V., Kompanets V.O., Kosareva O.G., Grigor'evskii A.V., Kandidov V.P. *Proc. SPIE*, **6733**, 67332I (2007).
23. Kompanets V.O., Chekalin S.V., Kosareva O.G., Grigor'evskii A.V., Kandidov V.P. *Quantum Electron*., **36**, 821 (2006) [*Kvantovaya Elektron*., **36**, 821 (2006)].
24. Faccio D., Rubino E., Lotti A., Couairon A., Dubietis A., Tamosauskas G., Papazoglou D.G., Tzortzakis S. *Phys. Rev. A*, **85**, 033829 (2012).
25. Dubietis A., Polesana P., Valiulis G., Stabinis A., Di Trapani P., Piskarskas A. *Opt. Express*, **15**, 4168 (2007).
26. Babin A.A., Kisilev A.M., Pravdenko K.I., Sergeev A.M., Stepanov A.N., Khazanov E.A. *Phys. Usp*., **42**, 74 (1999) [*Usp. Fiz. Nauk*, **169**, 80 (1999)].
27. Yashunin D.A., Mal'kov Yu.A., Stepanov A.N. *Quantum Electron.*, **43**, 300 (2013) [*Kvantovaya Elektron*., **43**, 300 (2013)].
28. Yashunin D.A., Malkov Yu.A., Mochalov L.A., Stepanov A.N. *J. Appl. Phys.*, **118**, 093106 (2015).
29. Dota Krithika, Pathak Abhishek, Dharmadhikari J.A., Mathur D., Dharmadhikari A.K. *Phys. Rev. A*, **86**, 023808 (2012).
30. Majus Donatas, Dubietis Audrius. *J. Opt. Soc. Am. B*, **30**, 994 (2013).
31. Stuart B.C., Feit M.D., Rubenchik A.M., Shore B.W., Perry M.D. *J. Opt. Soc. Am. B*, **13**, 459 (1996).
32. Kaiser A., Rethfeld B., Vicanek M., Simon G. *Phys. Rev. B*, **61**, 11437 (2000).
33. Mao S.S., Quéré F., Guizard S., Mao X., Russo R.E., Petite G., Martin P. *Appl. Phys. A*, **79**, 1695 (2004).
34. Rohlfing M., Louie S.G. *Phys. Rev. Lett*., **81**, 2312 (1998).
35. Chekalin S.V., Kompanets V.O., Dormidonov A.E., Zaloznaya E.D., Kandidov V.P. *Quantum Electron.*, **47**, 252 (2017) [*Kvantovaya Elektron.*, **47**, 252 (2017)].
36. Chekalin S.V., Dokukina A.E., Dormidonov A.E., Kompanets V.O., Smetanina E.O., Kandidov V.P. *J. Phys. B: At. Mol. Opt. Phys.*, **48**, 094008 (2015).